

# A Wearable Multi-Modal Bio-Sensing System Towards Real-World Applications

Siddharth , Student Member, IEEE, Aashish N. Patel , Member, IEEE, Tzyy-Ping Jung , Fellow, IEEE, and Terrence J. Sejnowski, Life Fellow, IEEE

**Abstract**—Multi-modal bio-sensing has recently been used as effective research tools in affective computing, autism, clinical disorders, and virtual reality among other areas. However, none of the existing bio-sensing systems support multi-modality in a wearable manner outside well-controlled laboratory environments with research-grade measurements. This paper attempts to bridge this gap by developing a wearable multi-modal bio-sensing system capable of collecting, synchronizing, recording, and transmitting data from multiple bio-sensors: PPG, EEG, eye-gaze headset, body motion capture, GSR, etc., while also providing task modulation features including visual-stimulus tagging. This study describes the development and integration of various components of our system. We evaluate the developed sensors by comparing their measurements to those obtained by a standard research-grade bio-sensors. We first evaluate different sensor modalities of our headset, namely, earlobe-based PPG module with motion-noise canceling for ECG during heart-beat calculation. We also compare the steady-state visually evoked potentials measured by our shielded dry EEG sensors with the potentials obtained by commercially available dry EEG sensors. We also investigate the effect of head movements on the accuracy and precision of our wearable eye-gaze system. Furthermore, we carry out two practical tasks to demonstrate the applications of using multiple sensor modalities for exploring previously unanswerable questions in bio-sensing. Specifically, utilizing bio-sensing, we show which strategy works best for playing “Where is Waldo?” visual-search game, changes in EEG corresponding to true vs. false target fixations in this game, and predicting the loss/draw/win states through bio-sensing modalities while learning their limitations in a “Rock-Paper-Scissors” game.

**Index Terms**—Brain-computer interface (BCI), bio-sensing, EEG, pupillometry, multi-modality, PPG, eye-gaze, stimulus tagging, gaming.

Manuscript received June 28, 2018; accepted August 24, 2018. Date of publication September 4, 2018; date of current version March 19, 2019. This work was supported in part by the Army Research Laboratory under Cooperative Agreement Number W911NF-10-2-0022, NSF NCS-1734883, NSF 1540943, NSF IIP-1719130, and in part under a Grant from UC San Diego Center for Wearable Sensors. (Corresponding author: Siddharth.)

Siddharth is with the Department of Electrical and Computer Engineering, University of California San Diego, La Jolla, CA 92093 USA (e-mail: ssiddhar@eng.ucsd.edu).

A. N. Patel is with the Department of Electrical and Computer Engineering, University of California San Diego.

T.-P. Jung and T. J. Sejnowski are with the Institute for Neural Computation, University of California San Diego.

Digital Object Identifier 10.1109/TBME.2018.2868759

## I. INTRODUCTION

IN RECENT years, there have been many advances in the field of wearable bio-sensing. This trend has led to the development of multiple wearable bio-sensors capable of measuring galvanic skin response (GSR), photoplethysmogram (PPG), etc. integrated into portable form-factors such as smartwatches. The use of bio-signals for various applications such as robotics [1], [2], mental health [3], affective computing [4], human-computer interaction [5], [6] etc. has been expanding throughout the past decade. During the same time, the concept of using more than one bio-sensing modality has also gained popularity. This is primarily driven by the assumption that the limitations of a bio-sensor can be compensated by using another for specific applications. For example, since EEG provides good temporal resolution but poor spatial resolution it might be possible to use other modalities such as PPG and GSR to augment the performance in an emotion classification task rather than using EEG alone [7], [8].

Unfortunately, the integration of above-mentioned bio-sensing modalities is usually overlooked for more naturalistic research studies due to cost, bulk, and technical difficulty [9], [10]. A typical strategy used to measure multiple bio-signals in the real-world is to buy various sensors and then extract data from each of them separately. This setup, however, leads to unwieldy subject preparation and increased post-processing synchronization effort, both of which add sources of noise and inconvenience. Specifically, no integrated headset has been proposed to measure multiple bio-signals simultaneously in a synchronized manner. Without the possibility of simultaneous recordings from multiple modalities, it is difficult, if not impossible, to explore questions corresponding to changes in physiology while performing actions in the real world.

The problem of not being able to collect data in real-world environments is compounded by the lack of techniques to automatically recognize and tag real-life events or stimuli. The standard process employed for stimulus tagging requires an individual (experimenter) to manually tag the various stimuli from frame to frame in a video stream. This process is cumbersome, time-consuming, and laborious. Furthermore, the stimulus onset is not measured with fine-resolution or is ill-defined in such setups [11], [12]. A solution is to track eye-gaze to infer the stimulus onsets [13]. This allows pinpointing of the visual region, but still requires stimulus tagging.

Additionally, there is a design element associated with the bio-sensors, which needs to be optimized for compactness and

cost for any multi-modal bio-sensing system. Any such device has to be capable of synchronizing multiple data streams and should be packaged in a compact form factor for easy use. For example, the use of wet electrodes for measuring EEG or electrocardiogram (ECG), which may require placing sensors over the chest, is undesirable for real-world setups. This study addresses the above limitations by designing novel research-grade bio-sensors capable of measuring physiological measurements in real-world environments with automatic visual tagging and integrating the sensors in the form of a compact wearable headset. This research also presents evaluation on two “real-world” experiment setups through the use of gaming towards utilizing multiple sensor modalities. We show that previously unexplored physiological questions can be addressed using multiple sensor modalities.

## II. PROPOSED SYSTEM AND RELATED WORK

We designed and evaluated a novel earlobe-based, high-resolution PPG sensor that is capable of measuring heart rate and heart-rate variability as well as providing raw PPG data from the earlobe. Using adaptive noise cancellation and intentional placement at the earlobe to minimize sensor movement, the PPG sensor is capable of minimizing motion noise. We also designed and evaluated novel dry EEG sensors capable of actively filtering the EEG signals by shielding themselves from ambient electrostatic noise. These EEG sensors are used with a high-sampling and ultra-low-noise analog to digital converter (ADC) module. We also designed and evaluated a dual-camera-based eyeglass capable of measuring eye-gaze (overlaid on the subject’s field of view), pupillometry, fixations, and saccades. Data acquisition and synchronization from all these sensors is done using an embedded system. These data streams can then be saved on the device or wirelessly transmitted in real-time for visualization and analysis. The framework is designed to automatically tag visual stimuli in real-world scenarios with subject’s eye-gaze over the various bio-sensing modalities. Finally, the framework is scalable such that it can be expanded to support other bio-sensing modalities from the market. To the best of our knowledge, this is the only multi-modal bio-sensing system capable of working with such a wide range of research-grade sensors.

**Table I** compares our system with many existing state-of-the-art bio-sensing systems. Clearly, we can see that in all categories our system is more comprehensive and flexible than all the existing bio-sensing systems. The lack of cost comparison in the Table is because many of the systems including ours have not been commercialized into products. Hence, it is not a fair comparison to evaluate the retail prices of select systems with the fabrication costs of others.

In real-world applications, PPG has been substituted for ECG due to the ease it offers in measuring heart rate. It does not require using wet electrodes over the chest and can easily be integrated onto watches or armbands [10], [19]. But, it has its own limitations. First, most of the available PPG sensors do not have sampling rate high enough and fine ADC resolution to measure heart-rate variability (HRV) in addition to heart rate (HR). HRV

has been shown to be a good measure of emotional valence and physiological activity. Secondly, PPG sensors over the arm or wrist tend to be noisy because of the constant movements of the limbs while performing real-world tasks. On the other hand, PPG systems designed for the earlobe also suffer from noise due to walking or other head/neck movements [19]. In the rare case when noise filtering is used in PPG, the hardware design is bulky due to the large size of the circuit board used in the setup [20].

EEG sensors come in dry or wet-electrode based configurations. The wet electrodes either require the application of gel or saline water during the experiment and hence are not ideal outside laboratory environments [21]. The dry electrodes usually do not have a long service life since they are generally made of Ag/AgCl or gold (Au) coating over a metal, plastic or polymer, which tend to wear off [22], [23]. Furthermore, coating Ag/AgCl is a costly electrochemical process.

Eye-gaze tracking systems tend to be bulky and may even require the subject to place his/her face on a chin rest [24], [25]. Even when they are compact, these systems are not mobile and the subject has to be constantly in its field of view [26]. These limitations restrict their use outside well-controlled laboratories, where illumination varies and the subject is mobile at all times. Furthermore, all such systems only measure eye-gaze as being pointed over a display monitor and not in the real world. They are unable to overlay the gaze over the subject’s view if the display screen is not in his/her field of view. The solution is to use head-mounted eye-gaze systems but they tend to use a laptop instead of a small embedded system for processing and viewing the camera streams [27]. Thus, the laptop has to be carried in a bag, restricting the subject’s freedom of movement.

To tag the stimuli with various bio-sensing modalities, the norm has been to use a key/button press, fix the onset and order of stimuli on a display, or time it with a particular event etc. [11], [12] But, in real-world scenarios, such methods either cannot be used due to the mobile nature of the setup or induce a sense of uncertainty which has to be removed by manual tagging. Such manual tagging is laborious and time-consuming. The only viable solution is to tag stimuli automatically after recognizing them in the subject’s field of view. However, it lacks the knowledge of whether the subject was actually focusing on the stimuli or rather was looking at some other areas in his/her field of view.

The existing multi-modal experimental setups are tethered, are not compact and tend to just attach various sensors on the subject, which are then connected to one or more data acquisition systems [4], [9]. This further reduces the mobility for experiments outside laboratories. The use of independent clock for each of the different modality complicates the issue of synchronizing the various modalities. For real-time display, transmitting data streams from these sensors over Wi-Fi or Bluetooth may introduce varying latency. Thus, the only solution is to design a closely packed hardware system [28], which synchronizes the various data streams while acquiring them in a wired manner and using only one clock (that of the embedded system itself). The synchronized streams can then be either recorded or sent to a display screen which does not affect either the compact nature of hardware or synchronization in software framework.

TABLE I  
COMPARISON OF MULTI-MODAL BIO-SENSING SYSTEMS

Features	This System	iMotions [10]	Microsoft [16]	Biovotion [17]	Teaergo [18]	OpenBCI [19]	Imperial College [20]
Sensing Modalities	EEG, PPG, Eye-Gaze Tracking, Pupilometry	EEG, GSR, Eye-Tracking	ECG, EMG	PPG, GSR, Skin Temperature	PPG, GSR, Skin Temperature	EEG, EMG, GSR, Eye-Gaze, Motion Tracking	EEG, EMG, ECG
Fully integrated, self-contained module*	Yes	No, multiple modules	Yes	Yes	No, multiple modules	Yes	No, multiple modules
Wireless Synchronization†	Yes	Yes	No	No	Yes	No	No
Automatic Visual Stimuli Tagging	Yes	No	No	No	No	No	No
Noise canceling measures	Yes (ANC, Shielding)	No	No	No	No	No	No
Research grade‡	Yes	Yes	No	No	Yes	Yes	Yes
Performance Evaluation while in motion	Yes	No	Yes	Yes	Yes	No	No

\*Containing data acquisition, noise filtering, digitizing, transmission circuitry and battery.

†Capable of synchronizing with any external sensor too while transmitting wirelessly.

‡Capable of acquiring data with high bit resolution and high sampling rate.

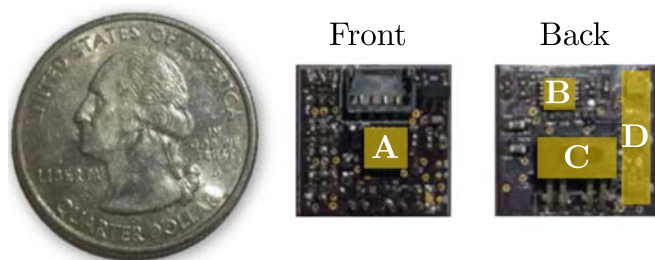


Fig. 1. The miniaturized PPG sensor with a scale reference. (A) 3-axis accelerometer. (B) 100 Hz 16-bit ADC. (C) IR emitter and receiver. (D) A third-order filter bank.

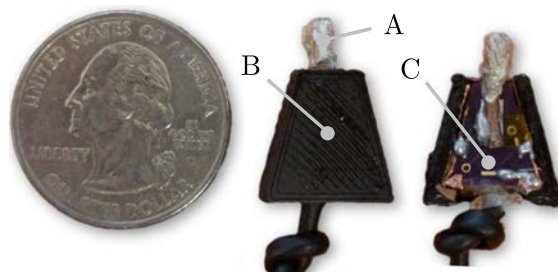


Fig. 2. The EEG sensor with a scale reference. (A) Silver (Ag) based conductive element. (B) 3D printed case housing a conductive element for shielding. (C) The amplifier circuitry.

In the next section, we present the various sensors and methods developed by us to address the above limitations.

### III. SYSTEM OVERVIEW

This section details the development of each of the sensor modules incorporated in our system with its features and the embedded system used for their integration.

#### A. Earlobe-Based PPG Sensor

We developed an earlobe-based PPG sensor. The PPG sensor module is very compact ( $1.6 \times 1.6 \times 0.6$  cm) and sandwiched to the earlobe using two small neodymium magnets. The PPG sensor module (Fig. 1) houses an Infrared (IR) emitter-detector (Vishay TCRT 1000) for measuring PPG, a 3-axis accelerometer (Analog Devices ADXL 335), a high-precision (16-bit) and high-sampling rate (100 Hz.) ADC (Texas Instruments ADS 1115), and a third-order analog high-gain band-pass filter (BPF, cutoff 0.8 - 4 Hz using three Microchip MCP6001 op-amps).

This PPG signal is then amplified using the high-gain band-pass filter and a relevant frequency band is extracted. The filtered PPG data along with accelerometer's data are digitized using the

ADC before transmission. Thus, the PPG module is capable of filtering the signal on-board (despite being so minuscule in size) and converting the signal to a digital format for the calculation of heart rate and heart-rate variability. The onboard accelerometer serves two purposes. First, it can be used to measure and monitor head movements because the sensor is fixed on the earlobe with reference to the position of the subject's face. Secondly, the accelerometer provides a measure of noise due to motion and removes it from the PPG signal using an adaptive noise-cancellation (ANC) filter. The filter [29] can be implemented inside our embedded system (section E) in real-time. The filter works by constructing a model of noise due to motion (such as while walking) from the reading of the accelerometer and reconstructing the noise-removed PPG signal.

#### B. EEG Sensors and Data Acquisition

We developed novel dry EEG sensors (Fig. 2) that can be easily adjusted under the hairs to measure EEG signals from the scalp. These EEG sensors consist of a highly conductive element made from silver (Ag) epoxy (electrical resistivity  $0.007 \Omega \cdot \text{cm}$ ). This silver-epoxy-based conductive element

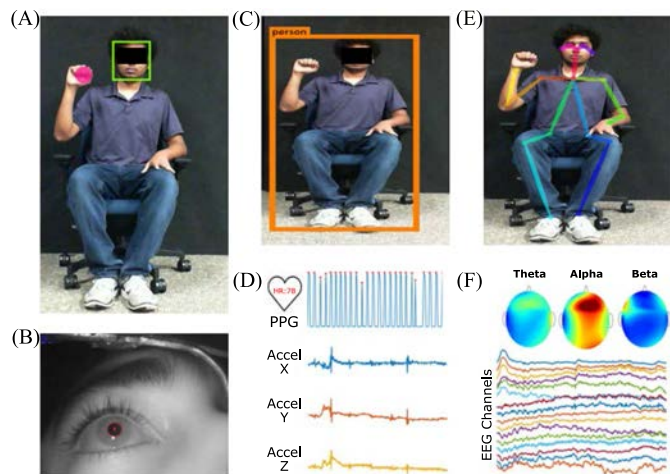


**Fig. 3.** Visualization of our software. (A) Eye-gaze overlaid on world view. (B) Detected pupil in IR eye camera image. (C) Object detection network. (D) PPG and accelerometer signals with noise canceling and heart-rate computation. (E) Human pose detection network. (F) EEG signals and power spectral density of three EEG bands.

provides the sensor a long life since the silver does not wear off as fast as it does on EEG sensors coated with Ag/AgCl. The sensor also has an on-board OpAmp (Texas Instruments TLV 2211) in a voltage-follower configuration to shield the EEG signal from noise by increasing the signal-to-noise ratio (SNR) of the EEG signal. Furthermore, the sensor is enclosed in a Faraday cage made of conductive copper foil tape. This shielding is used to remove external noise from the environment before the signal is digitized. For subjects with dense hair, a drop of saline water can be added to increase the conductance between the sensing element and the subject's scalp.

For converting the analog noise-removed EEG signal to a digital format, we designed an assembly for fine resolution (24-bit), high-sampling rate (up to 16k samples/second), ultra-low input referred noise (1  $\mu$ V) ADC (Texas Instruments ADS 1299). Our assembly is such that it employs a low-pass filter before the signal goes into the ADC, whose parameters such as sampling rate, bias calculation, internal source current amplitude for impedance measurement etc. can be controlled by the software [30], [31]. The assembly can support up to eight EEG channels (Fig. 5F) whereas the design of the board is such that multiple boards can be stacked to accommodate more EEG channels. We use two such boards in our headset to support 16 EEG channels (Fp1, Fp2, F7, F3, Fz, F4, F8, C3, Cz, C4, P3, Pz, P4, O1, Oz, and O2 according to the International 10-20 EEG placement). Continuous impedance monitoring is made for each electrode in real-time to assess the quality of the EEG signal and electrode placement. Furthermore, using Independent Component Analysis (ICA) [32], [33], various independent components of the signal can be separated to identify noise due to blink, eye movement, EMG, etc.

### C. Eye-Gaze and Pupillometry Sensors

We use two miniature cameras (Fig. 6) to assess the subject's eye-gaze location and pupillometry parameters such as the di-

ameter of the pupil, fixations, saccades etc. The eye camera consists of two infrared (IR) LED's (970 nm wavelength), which are used to illuminate the region around the eye. Because the LEDs are IR-based, the eye camera can detect the pupil under a wide variety of illumination conditions. We modified PupilLabs' pupil-detection and eye-gaze calibration software to detect the pupil and calibrate subject's gaze [27]. A display screen (i.e. laptop) is needed only for the initial eye-gaze calibration step, which is done using a manual selection of natural features in the field of view. The gaze is then superimposed on the subject's view from the world camera. Both cameras stream at 30 frames-per-second (fps) while the resolution can be adjusted as per the need of study.

### D. Stimulus Tagging

We use You Only Look Once (YOLO) deep-learning algorithm to automatically tag various stimuli in the feed from the world camera in real time [34]. The algorithm can be trained for custom object classes using large image databases with multiple classes depending on experimental needs (for example 80 object categories in COCO dataset with 300 K images). Whenever the subject's gaze falls inside the bounding box of one of the object classes (stimuli), the bio-sensing modalities are automatically tagged. Therefore, instead of manually tagging the stimuli during the experiment, our software automatically tags the salient information. Thus, for example, if the subject is looking at a person's face, his/her EEG can be time-synchronized to the gaze and analyzed to detect the level of arousal (Fig. 3). Due to the significant computational requirements of using YOLO, the stimulus tagging is done on a laptop (rather than the embedded system) in real-time or processed post-hoc. OpenPose [36] is used to automatically tag the human pose by detecting positions of the body joints. Lab Streaming Layer (LSL) [37] library is used to synchronize the data streams from the camera on the embedded system and stimulus tagging on the laptop.

### E. Embedded System Framework

Each of the above modalities is wired to a custom development board (Fig. 5), which uses an embedded system containing Broadcom BCM2837 processor. The board has the capability to attach a world camera, eye camera, PPG module, and EEG module. Additionally, the board houses a headphone jack which can be used for playing audio recordings during experiments. The clock on the embedded system is common for all modalities helping to ensure data synchronization from independent streams using LSL. This library allows for the spawning of a global clock which takes into account the relative difference between local clocks on the embedded system and laptop for synchronizing various data streams from the two devices in real-time. While sending the video streams wirelessly, we compress them using MJPEG compression. Fig. 4 shows the block diagram of the complete working architecture of our system, sensor components, data processing and transmission by Wi-Fi (using Realtek RTL 8723BS module). The system is powered using a small Li-Ion battery (Panasonic NCR18650B 3400 mAh), which lasts for approximately three hours when all sensor modalities

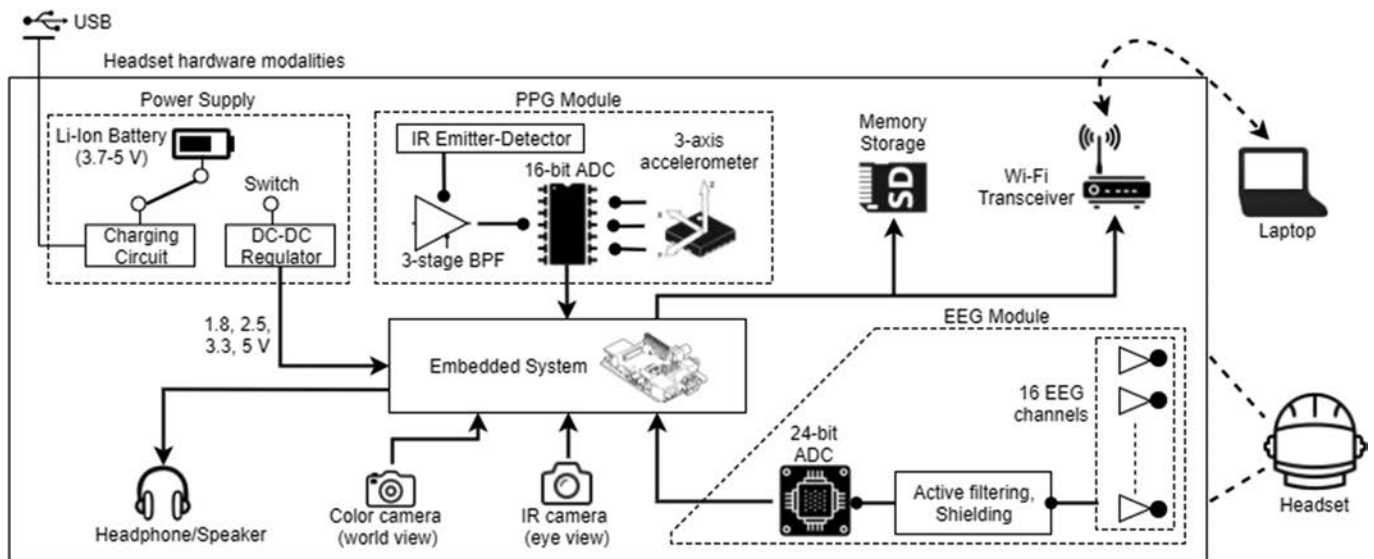


Fig. 4. Overview of the integrated system architecture.

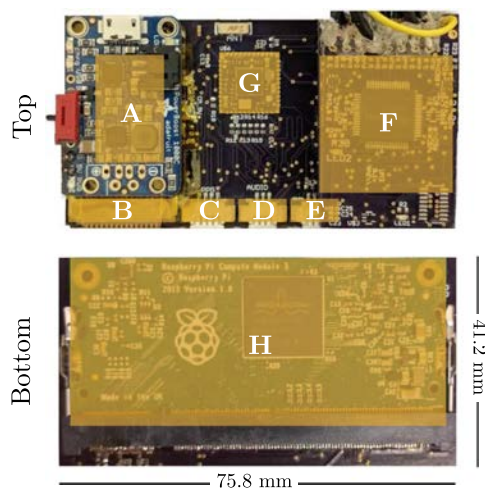


Fig. 5. Embedded system. (A) Power circuitry. (B) World camera connector. (C) PPG connector. (D) Audio jack connector. (E) Eye camera connector. (F) EEG sensors connector and ADC module. (G) Wi-Fi module. (H) Microprocessor module.

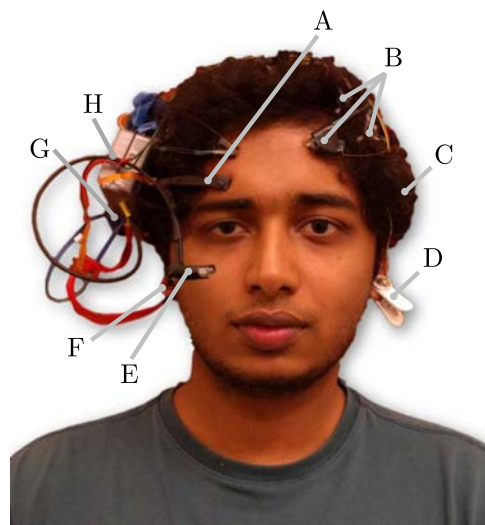


Fig. 6. Integrated headset. (A) World camera. (B) EEG sensors. (C) Battery. (D) EEG reference electrode. (E) Eye camera. (F) Earlobe PPG sensor. (G) Headphone/speaker connector. (H) Embedded system (The subject gave consent to use his face for publication).

are enabled. However, the system can also be powered by any compact 5V-output mobile power bank for more than eight hours of continuous use. In the future, we would explore increasing the battery life further by using low-power cameras and system-on-modules (SOMs).

#### IV. EVALUATION

To evaluate the efficacy of our integrated headset (Fig. 6), we evaluated the individual components on multiple subjects. Below we provide the evaluation results for each of the components. We then designed two experiment scenarios using commonly played games: “Where is Waldo?” and “Rock-Paper-Scissors” during which we collect multi-modal data using the evaluated sensor modalities. We then show how a fusion of in-

formation from individual modalities can provide new insights into human physiology. The human trial portion of our study was reviewed and approved by an IRB of University of California San Diego, and all subjects provided informed consent.

##### A. The Evaluation of Sensor Modalities

We use multiple benchmarks to evaluate each of the sensors developed in this study. The apparatus designed for evaluating these sensors also include various types of head and body movements to assess the effect of our noise-canceling techniques.

**1) Earlobe PPG:** The earlobe PPG module was evaluated during rest and active conditions. In particular, the feature of

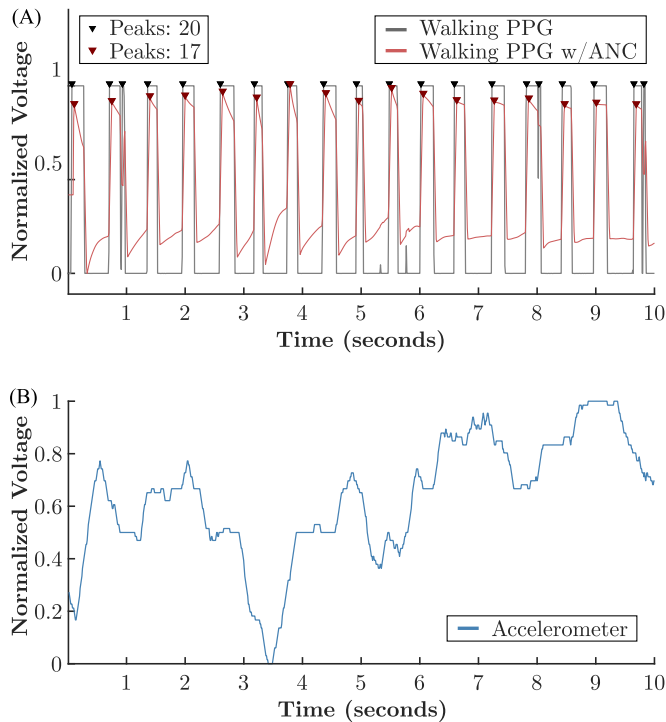


Fig. 7. Comparison of the 10-second waveforms from the earlobe PPG sensor before and after ANC during walking. (A) PPG without and after noise-cancellation. (B) Vertical acceleration used as the noise measure.

interest, heart rate, was measured while subjects were sitting and walking in place. The PPG sensor was placed on the earlobe as in Fig. 6 and measured the changes in blood volume at the sampling rate of 100 Hz. Simultaneously, the baseline was collected using an EEG/ECG acquisition system sampled at 1 KHz from the Institute of Neural Engineering, Tsinghua University, China. Three electrodes were placed on the subjects' chest over the heart, and on either side of the ribs.

Six subjects participated in eight different trials: four sitting and four walking, during which their ECG and PPG data were simultaneously measured. In each trial, two minutes of data were collected. For the walking condition, subjects were instructed to walk-in-place at a regular rate and ANC was performed to remove motion noise. We used a peak detection algorithm to find the heart beats in both signals for counting the heart rate.

Fig. 7 shows the working of the 10th order ANC filter utilized on a 10-second interval of PPG data while walking. The original PPG data (in blue) in Fig. 7A are clipped at the top because a third order high-gain band-pass filter was used thus amplifying the signal and making it easier to distinguish the peaks in PPG. As we can see from Fig. 7A, the number of peaks in the original waveform is computed to be 20, which is incorrect as the waveform is distorted. We then use the measure of the noise from vertical acceleration (Fig. 7B) for the ANC filter. Noise-removed PPG waveform with the use of ANC filter is shown in Fig. 7A and as expected the erroneous peaks are eliminated, giving the total number of peaks as 17.

We then performed Bland-Altman analysis [38], which is a general and effective statistical method for assessing the agree-

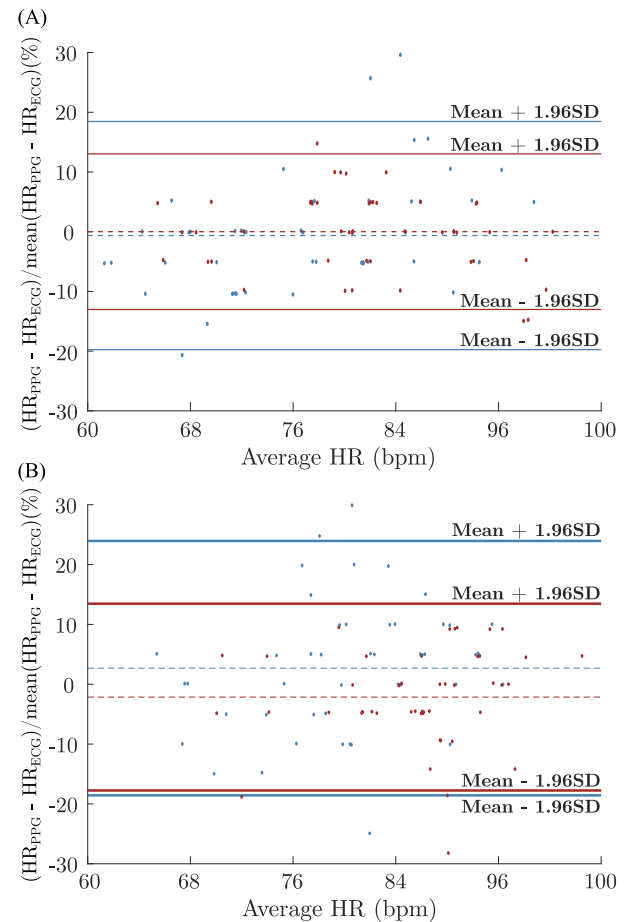
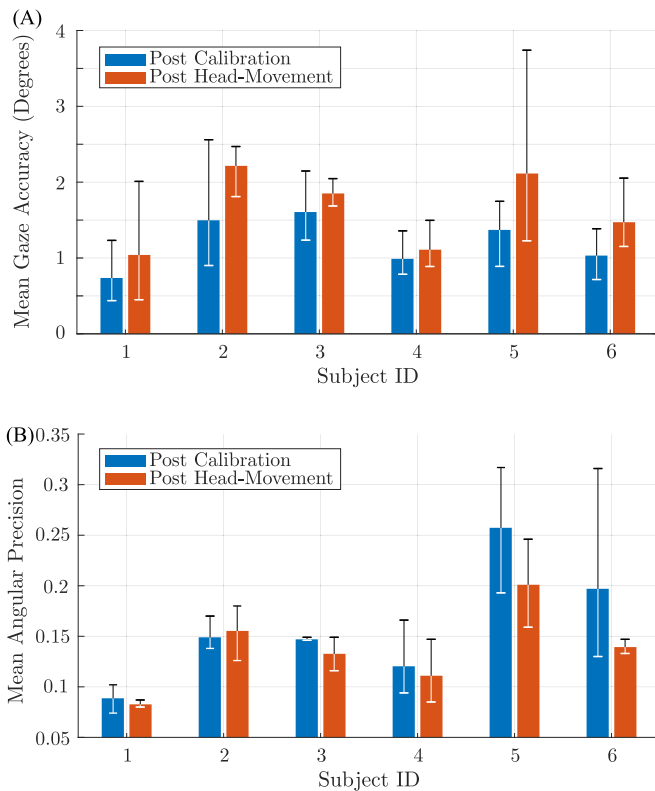


Fig. 8. PPG vs. ECG Bland-Altman evaluation (blue- before ANC, red- after using ANC). (A) While sitting. (B) While walking. Heart-rate computed by ANC filtered PPG conforms more closely to the true heart-rate.

ment between two clinical measurements to compare the heart rate obtained by our PPG module to the true heart rate computed using the high-resolution ECG signal. Fifteen-second trials were used to calculate the HR using the peak-detection algorithm. Fig. 8A shows the result of the Bland-Altman analysis while the subjects were sitting. As we can see from the figure, most of the trials are between the Mean  $\pm$  1.96SD agreement threshold for both, with and without using ANC. Further, we see that using ANC decreases the agreement threshold, making the two signals adhere to more conformity. We see similar results for the trials when subjects were walking (Fig. 8B) and again using ANC makes the HR measures from the two signals more agreeable. Furthermore, for both cases, the trials from the two signals were almost always in agreement, indicating that our earlobe PPG module is capable of measuring heart rate with high accuracy.

**2) Eye Gaze Evaluation:** The performance of the paired eye-pupil monitoring and world-view cameras in measuring eye gaze were evaluated using a structured visual task to measure precision and accuracy during use. We measured the gaze accuracy and precision for subjects following calibration (an ideal setting) and after head movements (a real-world use). In this task, we asked the subjects to calibrate their eye gaze using nine



**Fig. 9.** (A) Gaze accuracy (average angular offset between fixation locations and corresponding targets) evaluation. (B) Gaze precision (root-mean-square of the angular distance between successive samples during fixation) evaluation. For both metrics, this system performs as well or better than such existing ones.

targets which appeared on a screen 2.5 feet away from them (such that  $>90\%$  of the camera’s field of view was composed of the task-screen). For six subjects, we used a series of 20 unique targets randomly distributed on the screen to account for the majority of their field of view. Thus, this composed the accuracy and precision measurements just after calibration. We then asked the participants to move their head naturally for 30 seconds without removing the headset. This action was designed to simulate the active head-movement scenarios when wearing the headset because usually the gaze performance is not reported after the subject has moved from his/her position. Similar to the above task, we asked the subjects to again gaze at 20 different points appearing on the screen to assess the gaze performance after head movements. The above process was repeated three times for each subject. Importantly, we did not use any chin rest during or after calibration so that gaze performance is measured with natural head and body movements.

The accuracy is measured as the average angular offset - distance in degrees of the visual angle - between fixation locations and the corresponding fixation targets. Fig. 9A shows the gaze accuracy obtained before and after head movements. The mean gaze accuracy over all the trials was found to be 1.21 degrees without and 1.63 degrees after head movements. The decrease in gaze accuracy after head movements is expected because the headset’s position is displaced albeit by a small value. For all the subjects, the mean gaze accuracy was mostly less than 2 de-

grees and the mean performance drifts only 0.42 degree, which is significantly less than 1–2 degree drift in commercially available eye-gaze systems [24]. The precision is measured as the root-mean-square of the angular distance between successive samples during a fixation. Fig. 9B shows the results of the angular precision for all the subjects. The mean angular precision was found to be 0.16 and 0.14 before and after head movements respectively. As is clear from the figure, the degree of visual angle is almost always within the range of  $\pm 0.15$ . Furthermore, the precision has a mean shift post head movement of only 0.2, indicating a minimal angular distance shift comparable to existing systems.

**3) EEG Sensors Evaluation:** For the evaluation of our EEG sensors, the comparison was two-fold. First, we compared our EEG sensor with the state-of-the-art dry EEG sensors by Cognionics [23] to evaluate the signal correlation achieved using the two types of sensors. This also proves to be a test of whether our EEG sensors are actually acquiring EEG as opposed to just electromagnetic noise, and if they are able to shield themselves from ambient noise in the environment. Second, we evaluated our sensors on a steady-state visually evoked potentials (SSVEP) BCI task to evaluate their performance in measuring various frequencies during standard use.

For the SSVEP testing, we used five of our EEG sensors placed at T5, O1, Oz, O2, and T6 sites according to the standard EEG 10–20 system. The location over and near the occipital lobe was chosen to evaluate the performance of our sensors because the SSVEPs in response to repetitive visual stimuli of different frequencies are strongest over the occipital lobe. Ten subjects participated in this experiment constituting three trials of ten random numbers each to be typed using an SSVEP-based keypad on a mobile tablet (Samsung Galaxy S2) with an EEG sampling rate of 500 Hz. The frequencies of the 12 stimuli on the keypad (BCI speller) varied between 9–11.75 Hz with increments of 0.25 Hz. This fine resolution in increment was chosen to assess the capability of sensors in distinguishing between minutely varying frequencies. The stimulus presentation time was 4 seconds with an interval of 1 second of a blank screen between two consecutive stimuli. We only used the middle 2 seconds of data from each trial for SSVEP analysis. To compare the signal quality obtained from the two types of sensors, we used Cognionics sleep headband to acquire EEG from one Cognionics sensor at the temporal lobe and one of our sensors next to it. The location was chosen so that hairs on the scalp are present around the sensors.

Fig. 10A plots 4-second of EEG data acquired by the two sensors where a high correlation between the two signals is evident and almost always they follow a pattern. Fig. 10B plots the correlation of a subset of 12 of the total trials. The correlations between the EEG signals acquired by the two different sensors were very high (the mean correlation reached 0.901), indicating that the dry EEG sensor developed in this study is capable of measuring EEG signals from the hair-covered scalp areas.

As mentioned above, each subject needed to ‘type’ ten digits in each of the three trials. We computed the SSVEP classification performance (Fig. 11) using the filter-bank correlation analysis [39], [40]. This method does not require any training and is

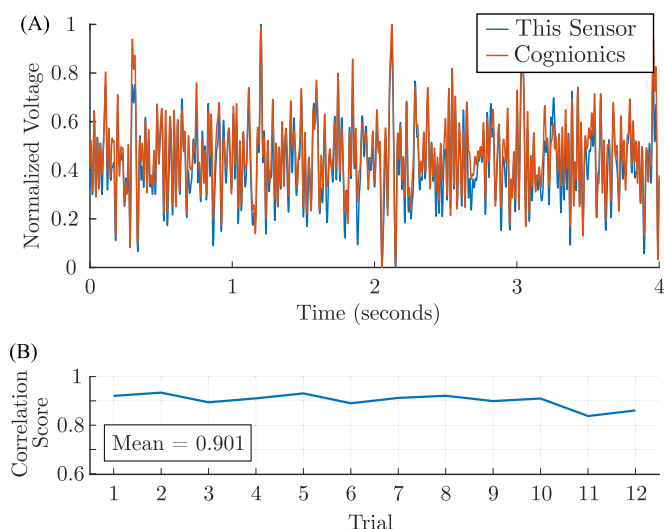


Fig. 10. (A) A comparison of 4-second EEG signals acquired by the proposed and Cognionics dry EEG sensors. (B) Correlation score between the EEG recorded from the two sensors. Recordings from both the sensors show very high correlation.

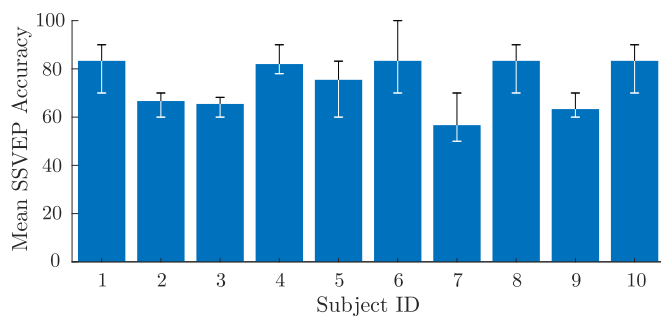


Fig. 11. SSVEP accuracy plot for 0.25Hz increments in stimulus frequencies. Even for small increments of 0.25 Hz we see high SSVEP accuracy across subjects.

capable of working in real time. As mentioned above, we only used the middle two seconds of EEG data during the 4-second stimulus presentation for evaluation. For almost all the subjects, the performance of SSVEP accuracy was very good ( $\sim 80\%$  accuracy). There were some expected variations because it is well known that the signal-to-noise ratio of SSVEPs varies among individuals. The mean performance across all the subjects was 74.23%.

### B. Multi-modal Evaluation in “Real-World” Scenarios

We designed two experiments in which ten subjects participated to play two games. For the “Where is Waldo?” game, the 30th anniversary book of the series was used which contains thirteen different scenes (trials) in which the target (“Waldo”) has to be searched for. This experiment scenario was chosen because it allows for analyzing gaze-related fixations and patterns. While searching for the target, many non-targets are present and hence target vs. non-target event-related potential (ERP) can also be assessed. The book was placed at a distance of about 20 inches from the subjects who were seated and equipped with the sensor modalities mentioned above. The subjects were asked to

search for the target without any time constraints. The researcher pressed a button before each trial and asked the subjects to start searching for the target. The subject conveyed that s/he has found the target verbally by saying “Found”. Between each trial, the researcher flipped the page of the book to the next scene.

In the “Rock-Paper-Scissors” game, the researcher was seated in front of the subject (see Fig. 3A). A sound beep every 17 seconds signaled the start of a trial. For each subject, the game was played for 50 trials. The first two seconds after the sound beep were used to play the game whereas next fifteen seconds the subject was asked to rest. The subject was instructed to only play the game from his/her wrist and not twist the whole arm to avoid any headset movement. During the game-play, motivational phrases such as “Come on! You can still win.”, “Watch out! I will now make a comeback”, etc. were utilized to ensure continual subject motivation. After each trial, the researcher marked the outcome (win/loss/draw) for the subject by pressing a button. The choice of this game was made to analyze the changes in human physiology, particularly EEG and cardiac signals during the perception of winning/losing a game. These changes might be closer to positive/negative valence in emotional states but much more reliable since winning/losing are independent of one’s likes and dislikes that influences his/her emotions.

1) *Gaze-fixation Pattern vs. Time Taken in Finding the Target:* Different subjects used different strategies while searching for the target and hence we aim to study that which strategy works best for this type of gaming paradigm by investigating the subjects’ eye-gaze fixations across the trials. We plot (in ascending order) the average time taken by the subjects to find the target across the thirteen trials for the first visual-search experiment in Fig. 12A. Clearly, we can see three distinct groups of subject strategies marked by different colors based on the average time taken by them. These groups were formed statistically taking 33rd and 66th percentile of the data as boundaries. Such a wide distribution is understandable since subjects use different strategies to find the visual target. Some subjects start looking for the target in small portions of the whole page while moving slowly towards previously unexplored parts whereas others tend to randomly scan the available page with longer distances between successive fixations.

To exclude the data associated with eye blinks (i.e. eye closures) we imposed a confidence threshold of 70% in our pupil detection algorithm. Then, we used the Euclidean distance of 25 pixels as the maximum inter-sample distance and 500 milliseconds as the minimum fixation duration to find all the fixations associated with the trials for all the subjects. We then computed the median (more robust than mean since a single large distance between successive fixations would skew the mean) distance between successive fixations for the three groups of subjects and plot it in Fig. 12B. The median distance between successive fixations tends to increase in the same manner for the three groups as the average time taken by them increases. Fig. 12C shows an example of 30-seconds of gaze data of one subject each from the three groups. As is clear from these figures, the subjects in Group 1 tend to search for the target in small sections of the page whereas the subjects in Group 3 search for the target randomly across the whole page. Because subjects in

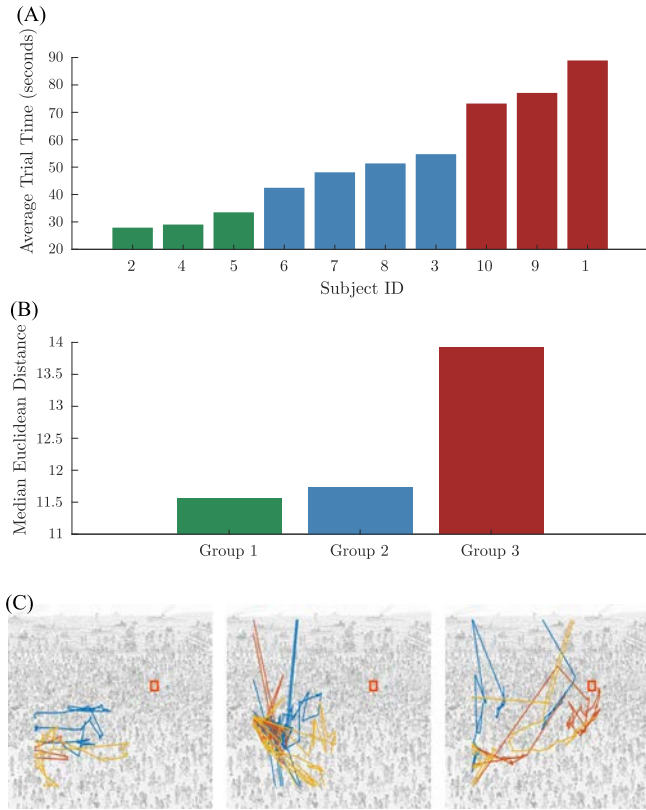


Fig. 12. (A) Average time taken by subjects across trials. (B) Median distance between fixations for the three subject groups. (C) Example of 30-seconds of gaze fixation data from one subject in each group (red, blue and yellow colors each represent 10-seconds of successive gaze data while target is marked with a box in the background). Subjects who traverse the page in small steps (as can be seen from the gaze fixation locations) are able to find the target faster.

Group 1 were able to find the target in the least time (on average), we believe that for “Where is Waldo?” game the best strategy is to focus on small portions of the page rather than searching for the target randomly across the whole page. It was impossible to gauge this insight without the use of eye-gaze tracker in which the subjects’ gaze can be overlaid on the image from the world camera in addition to detecting the pupil’s location with another camera.

**2) Fixation-related Potentials (FRP) Analysis:** EEG corresponding to fixations to the targets and non-targets while searching for the target in the “Where is Waldo?” game should represent distinct FRPs associated with the change in physiology. To discover this relationship, for each trial, we band-pass-filtered the EEG data within the trial between 1–30 Hz. We take the mean of 200 ms of data before each fixation as the baseline and subtract it from one-second of post-fixation EEG data to remove the variations in amplitude. We then calculated the FRP by averaging the data across the trials and subjects for all fixations greater than or equal to one second. We expect to see distinct FRPs for targets and non-targets. Fig. 13 plots the averaged FRPs for Fz and Oz EEG channels. The FRPs show distinct variations after the onset of the fixations at zero seconds; the characteristic large peak at 200 ms i.e. VPP and the trough between 200 and 400 ms i.e. N2 are consistent with the earlier

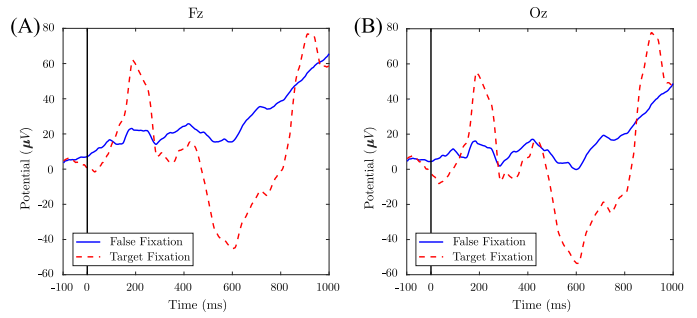


Fig. 13. FRP plot of two EEG channel locations. (A) Fz. (B) Oz. Target-fixed gaze FRP has much clear response than false-fixed gaze FRP.

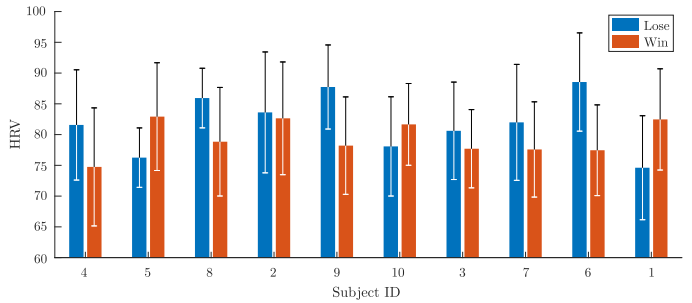


Fig. 14. Mean HRV variation across subjects arranged in ascending order of number of trials won.

findings that VPP and N2 components are associated with the face stimuli [41], [42]. Furthermore, a large P3 response almost at the rightmost part of the plot is associated with decision making and is clearly much larger for the target than the non-targets [43]. This is understandable because while searching for the target’s face, there are many non-targets with the similar face and clothing as the true target. When the subject first fixated on the true target, it takes time for him/her to assure it is indeed the true target. The slightly smeared nature of the P3 response is likely due to the fact that the latency of the P3 can vary across trials and individuals and the FRPs are time-locked to the onset of fixation, which is dependent on at what instant the fixation is detected by the algorithm since the pupil is continuously in motion. Our results show that combining eye-gaze and EEG provides insight into the search patterns and their effects on the EEG in a visual-search task. Another significant aspect of our apparatus was to use the book in a naturalistic setup, which allows unconstrained head/body movements rather than asking the subjects search the face in front of a computer screen with their head positioned on a chin-rest.

**3) Variation Across HRV During Win/Loss:** HRV can be a reliable indicator of human emotions and mental states [8] and we wanted to see the variation across the subjects for the trials they won versus the ones they lost in the “Rock-Paper-Scissors” game. We computed HRV using the pNN50 algorithm [44] from 15-seconds of data for each trial. Fig. 14 shows the variation in HRV for all the subjects arranged by the number of trials won by them in ascending order. Based on the final score where Loss/Draw/Win corresponded to  $-1/0/1$  points, subjects 4 and 5 lost the game, subject 8 tied the game and the

TABLE II  
MODALITY PERFORMANCE FOR MULTI-MODAL CLASSIFICATION

Subject ID	1	2	3	4	5	6	7	8	9	10	Mean	Max	Std.
<b>Classification Performance (Loss/Draw/Win) Chance Accuracy: 33%</b>													
EEG (1-sec)	56	56	52	54	62	56	54	46	52	50	<b>53.80</b>	<b>62</b>	<b>4.26</b>
PPG (15-sec)	58	58	60	46	46	48	54	58	56	52	<b>53.60</b>	<b>60</b>	<b>5.32</b>
EEG + PPG (15-sec)	54	54	52	52	56	54	56	52	54	54	<b>53.80</b>	<b>56</b>	<b>1.48</b>
<b>Classification Performance (Loss/Win) Chance Accuracy: 50%</b>													
EEG (1-sec)	87.88	80.65	86.84	70.97	63.33	81.82	72.73	70.00	68.97	72.41	<b>75.56</b>	<b>87.88</b>	<b>8.21</b>
PPG (15-sec)	87.88	87.10	86.84	70.97	70.00	81.82	75.76	86.67	75.86	72.41	<b>79.53</b>	<b>87.88</b>	<b>7.30</b>
EEG + PPG (15-sec)	84.85	87.10	81.58	80.65	70.00	81.82	72.73	73.33	68.97	68.97	<b>77.00</b>	<b>87.10</b>	<b>6.92</b>

Leave one subject out validation was performed. All values denote percentage accuracy.

remaining subjects won the game from the researcher. Fig. 14 shows that for all the subjects except one (subject 2) there is an unmistakable difference between the values of averaged HRV for winning and for losing the trials, indicating that cardiac measures such as HRV can be helpful in distinguishing between physiological states corresponding to win vs. loss situations. Additionally, we see that different subjects respond differently to win/loss. For example, subjects 1, 5 and 10 show increase in averaged HRV for the trials they won whereas others show a decrease in HRV. This might mean that different subjects react differently to the situation when they are winning or losing the game i.e. some might be enjoying the experience of the game whereas others might be under stress to come up with techniques to win the game.

**4) Using Machine Learning to Predict the Results of the Gaming:** The aims of this evaluation are twofold. First, we are interested in studying how well the bio-sensing modalities can predict i.e. classify the result of a game trial utilizing changes in physiology for a new subject, and what are their limitations in temporal frequency domain i.e. for how long the data from a modality is required. Second, we want to see the potential benefits of combining features from different modalities in terms of accuracy and consistency. We used EEG and PPG to predict the outcome of a trial through these bio-sensing modalities. From the 500 total trials (50 each for 10 subjects), there were 137/183/180 trials for loss/draw/win respectively. We divided the result of each trial into two- (win/loss) and three (win/draw/loss) classes. We computed conditional entropy features [45] between each possible pairs of eight EEG electrodes. Hence, 28 EEG features were computed which were reduced to 20 components using Principal Component Analysis [46]. These features have been shown to work well for emotional valence and arousal classification [8]. We tried with various durations for the EEG data and found that 1-second of EEG data post-trial gives the best performance results. For PPG, in addition to the HRV features described above, we computed six statistical features [47]. The resultant seven features computed from 15 seconds of the PPG data were used for training the classifier. We performed leave-one-subject-out validation i.e. training data from 9 subjects and testing it for the remaining subject. Hence, since there are 50 game trials for each subject, 450 samples were used for training and 50 samples were used for testing. We used extreme learning machines (ELM) with a single hidden layer for training the classification model [48].

Table II shows the results for 2-class and 3-class classification performance for each subject and both the sensor modalities. For all cases and subjects, we see that the classification performance i.e. mean accuracy is well above the chance accuracy level. The maximum accuracy goes up to 62% for three classes (loss/draw/win) and 87.88% for two classes (loss/win). Interestingly, PPG works as well as EEG for three classes and even better than EEG for two-class classification despite being only a single-channel signal with fewer features. However, PPG changes were slow (here 15 seconds of data being used) and thus do not provide as good temporal resolution as EEG. Hence, if the trials would have been spaced closer in time (say only 5 seconds apart), it would not have been possible to classify the trial result using PPG because of the inability to compute HRV and other cardiac features in such a short time window. Whereas, EEG can perform well on a shorter timescale but needs more channels. When we used both modalities (by taking 15-seconds of EEG data), we found that the performance is not that much affected but the standard deviation significantly decreases. This means that using multiple modalities can help in producing consistent results across subjects because the fusion of features is able to compensate for the limitations of a single modality. Hence, using multiple modalities is good in both ways i.e. it gives the advantage to choose the modality as per the temporal resolution requirement or multiple modalities can be used together for more consistent performance across subjects.

## V. CONCLUSION

Bio-sensing technology is advancing rapidly both as a clinical research tool and applications in real-world settings. The existing bio-sensing systems are numerous and capable of measuring various physiological metrics in well-controlled laboratories. But, they are not practical for routine use by users in unconstrained real-world environments. Repeatedly, it has been shown that using multiple bio-sensing modalities improves performance and robustness of decoding brain states and responses to cognitively meaningful real-life events. Hence, developing a research-grade wearable multi-modal bio-sensing system would allow us to study a wide range of previously unexplored research problems in real-world settings similar to the two gaming paradigms we presented in this research work. Finally, this work presented a novel use of multiple bio-sensing modalities on “real-world” data while exploring previously unanswered questions in this area.

## REFERENCES

- [1] C. Breazeal, "Emotion and sociable humanoid robots," *Int. J. Human-Comput. Stud.*, vol. 59, no. 1, pp. 119–155, 2003.
- [2] C. J. Bell *et al.*, "Control of a humanoid robot by a noninvasive brain-computer interface in humans," *J. Neural Eng.*, vol. 5, no. 2, pp. 214–220, 2008.
- [3] P. D. Bamidis *et al.*, "Affective computing in the era of contemporary neurophysiology and health informatics," *Interacting Comput.*, vol. 16, no. 4, pp. 715–721, 2004.
- [4] W. Liu *et al.*, "Multimodal emotion recognition using multimodal deep learning," 2016, arXiv:1602.08225.
- [5] K. LaFleur *et al.*, "Quadcopter control in three-dimensional space using a noninvasive motor imagery-based brain-computer interface," *J. Neural Eng.*, vol. 10, no. 4, 2013, Art. no. 046003.
- [6] T. Carlson and J. d. R. Millan, "Brain-controlled wheelchairs: A robotic architecture," *IEEE Robot. Automat. Mag.*, vol. 20, no. 1, pp. 65–73, Mar. 2013.
- [7] S. Koelstra *et al.*, "DEAP: A database for emotion analysis; using physiological signals," *IEEE Trans. Affective Comput.*, vol. 3, no. 1, pp. 18–31, Jan.–Mar. 2012.
- [8] S. Siddharth *et al.*, "Multi-modal approach for affective computing," 2018, arXiv:1804.09452.
- [9] J. Lei *et al.*, "Identifying correlation between facial expression and heart rate and skin conductance with iMotions biometric platform," *J. Emerg. Forensic Sci. Res.*, vol. 2, no. 2, pp. 53–83, 2017.
- [10] G. Udovii *et al.*, "Wearable emotion recognition system based on GSR and PPG signals," in *Proc. 2nd Int. Workshop Multimedia Pers. Health Care*, Oct. 2017, pp. 53–59.
- [11] J. E. Kamienskowski *et al.*, "Fixation-related potentials in visual search: A combined EEG and eye tracking study Fixation-related potentials in visual search," *J. Vis.*, vol. 12, no. 7, 2012, Art. no. 4.
- [12] L. Ackualagna and B. Benjamin, "Gaze-independent BCI-spelling using rapid serial visual presentation (RSVP)," *Clin. Neurophysiol.*, vol. 124, no. 5, pp. 901–908, 2013.
- [13] M. Soleymani *et al.*, "A multimodal database for affect recognition and implicit tagging," *IEEE Trans. Affective Comput.*, vol. 3, no. 1, pp. 42–55, Jan.–Mar. 2012.
- [14] R. Rawassizadeh *et al.*, "Wearables: Has the age of smartwatches finally arrived?" *Commun. ACM*, vol. 58, no. 1, pp. 45–47, 2015.
- [15] T. Wyss *et al.*, "The comfort, acceptability and accuracy of energy expenditure estimation from wearable ambulatory physical activity monitoring systems in soldiers," *J. Sci. Med. Sport*, vol. 20, pp. S133–S134, 2017.
- [16] G. D. S. Bertolaccini *et al.*, "The influence of axle position and the use of accessories on the activity of upper limb muscles during manual wheelchair propulsion," *Int. J. Occupational Saf. Ergonom.*, vol. 24, pp. 311–315, 2017.
- [17] H. Suryotrisongko and F. Samopa, "Evaluating OpenBCI spiderclaw V1 headwear's electrodes placements for brain-computer interface (BCI) motor imagery application," *Procedia Comput. Sci.*, vol. 72, pp. 398–405, 2015.
- [18] W. Von Rosenberg *et al.*, "Smart helmet: Wearable multichannel ECG and EEG," *IEEE J. Translational Eng. Health Med.*, vol. 4, 2016, Art. no. 2700111.
- [19] J. A. C. Patterson *et al.*, "A flexible, low noise reflective PPG sensor platform for ear-worn heart rate monitoring," in *Proc. IEEE 6th Int. Workshop Wearable Implantable Body Sensor Netw.*, 2009, pp. 286–291.
- [20] M. Z. Poh *et al.*, "Motion-tolerant magnetic earring sensor and wireless earpiece for wearable photoplethysmography," *IEEE Trans. Inf. Technol. Biomed.*, vol. 14, no. 3, pp. 786–794, May 2010.
- [21] M. Duvinage *et al.*, "Performance of the Emotiv Epoc headset for P300-based applications," *Biomed. Eng. Online*, vol. 12, no. 1, 2013, Art. no. 56.
- [22] Y. M. Chi *et al.*, "A practical mobile dry EEG system for human computer interfaces," in *Proc. Int. Conf. Augmented Cognit.*, Jul. 2013, pp. 649–655.
- [23] Y. M. Chi *et al.*, "Dry and noncontact EEG sensors for mobile brain-computer interfaces," *IEEE Trans. Neural Syst. Rehabil. Eng.*, vol. 20, no. 2, pp. 228–235, Mar. 2012.
- [24] D. W. Hansen and J. Qiang, "In the eye of the beholder: A survey of models for eyes and gaze," *IEEE Trans. Pattern Anal. Mach. Intell.*, vol. 32, no. 3, pp. 478–500, Mar. 2010.
- [25] F. W. Cornelissen *et al.*, "The Eyelink Toolbox: Eye tracking with MATLAB and the Psychophysics Toolbox," *Behav. Res. Methods, Instrum., Comput.*, vol. 34, no. 4, pp. 613–617, 2002.
- [26] J. D. Morgante *et al.*, "A critical test of temporal and spatial accuracy of the Tobii T60XL eye tracker," *Infancy*, vol. 17, no. 1, pp. 9–32, 2012.
- [27] M. Kassner *et al.*, "Pupil: An open source platform for pervasive eye tracking and mobile gaze-based interaction," in *Proc. ACM Int. Joint Conf. Pervasive Ubiquitous Comput., Adjunct Publication*, Sep. 2014, pp. 1151–1160.
- [28] P. Siddharth *et al.*, "An affordable bio-sensing and activity tagging platform for HCI research," in *Proc. Int. Conf. Augmented Cognit.*, Jul. 2017, pp. 399–409.
- [29] B. Widrow *et al.*, "Adaptive noise cancelling: Principles and applications," *Proc. IEEE*, vol. 63, no. 12, pp. 1692–1716, Dec. 1975.
- [30] J. A. Lovelace *et al.*, "Modular, bluetooth enabled, wireless electroencephalograph (EEG) platform," in *Proc. IEEE 35th Annu. Int. Conf. Eng. Med. Biol. Soc.*, Jul. 2013, pp. 6361–6364.
- [31] E. Mastinu *et al.*, "Analog front-ends comparison in the way of a portable, low-power and low-cost EMG controller based on pattern recognition," in *Proc. IEEE 37th Annu. Int. Conf. Eng. Med. Biol. Soc.*, Aug. 2015, pp. 2111–2114.
- [32] S.-H. Hsu *et al.*, "Online recursive independent component analysis for real-time source separation of high-density EEG," in *Proc. IEEE 36th Annu. Int. Conf. Eng. Med. Biol. Soc.*, 2014, pp. 3845–3848.
- [33] S. Makeig *et al.*, "Independent component analysis of electroencephalographic data," *Adv. Neural Inf. Process. Syst.*, vol. 8, pp. 145–151, 1996.
- [34] J. Redmon *et al.*, "You only look once: Unified, real-time object detection," in *Proc. IEEE Conf. Comput. Vis. Pattern Recognit.*, 2016, pp. 779–788.
- [35] M. Everingham *et al.*, "The pascal visual object classes (VOC) challenge," *Int. J. Comput. Vis.*, vol. 88, no. 2, pp. 303–338, 2010.
- [36] Z. Cao *et al.*, "Realtime multi-person 2D pose estimation using part affinity fields," in *Proc. IEEE Conf. Comput. Vis. Pattern Recognit.*, Jul. 2017, vol. 1, Art. no. 7.
- [37] C. Kothe, "Lab streaming layer (LSL)," [Online]. Available: <https://github.com/scen/labstreaminglayer>. Accessed on: Oct. 26, 2015.
- [38] D. G. Altman and J. M. Bland, "Measurement in medicine: The analysis of method comparison studies," *Statistician*, vol. 32, pp. 307–317, 1983.
- [39] X. Chen *et al.*, "Filter bank canonical correlation analysis for implementing a high-speed SSVEP-based brain-computer interface," *J. Neural Eng.*, vol. 12, no. 4, 2015, Art. no. 046008.
- [40] X. Chen *et al.*, "High-speed spelling with a noninvasive brain-computer interface," *Proc. Nat. Academy Sci.*, vol. 112, no. 44, pp. E6058–E6067, 2015.
- [41] H. Wang *et al.*, "Convolutional neural network for target face detection using single-trial EEG signal," in *Proc. 2018 40th Annu. Int. Conf. Eng. Med. Biol. Soc.*, 2018.
- [42] J. M. Kaufmann *et al.*, "N250 ERP correlates of the acquisition of face representations across different images," *J. Cognitive Neurosci.*, vol. 21, no. 4, pp. 625–641, 2009.
- [43] J. Polich, "Updating P300: An integrative theory of P3a and P3b," *Clinical Neurophysiol.*, vol. 118, no. 10, pp. 2128–2148, 2007.
- [44] D. J. Ewing *et al.*, "New method for assessing cardiac parasympathetic activity using 24 hour electrocardiograms," *Heart*, vol. 52, no. 4, pp. 396–402, 1984.
- [45] H. Peng *et al.*, "Feature selection based on mutual information criteria of max-dependency, max-relevance, and min-redundancy," *IEEE Trans. Pattern Anal. Mach. Intell.*, vol. 27, no. 8, pp. 1226–1238, Aug. 2005.
- [46] S. Wold *et al.*, "Principal component analysis," *Chemometrics Intell. Laboratory Syst.*, vol. 2, no. 1–3, pp. 37–52, 1987.
- [47] K. Mera and T. Ichimura, "Emotion analyzing method using physiological state," in *Knowledge-Based Intelligent Information and Engineering Systems*. Berlin, Germany: Springer, 2004, pp. 195–201.
- [48] G. B. Huang *et al.*, "Extreme learning machine: Theory and applications," *Neurocomputing*, vol. 70, no. 1–3, pp. 489–501, 2006.